IEEE Access
Multidisciplinary | Rapid Review | Open Access Journal

SPECIAL SECTION ON MILLIMETER-WAVE AND TERAHERTZ PROPAGATION, CHANNEL MODELING AND APPLICATIONS

Received September 5, 2019, accepted September 20, 2019, date of publication October 2, 2019, date of current version October 30, 2019.

Digital Object Identifier 10.1109/ACCESS.2019.2945042

Measurement-Based Characterization of 39 GHz Millimeter-Wave Dual-Polarized Channel Under Foliage Loss Impact

YEJIAN LV[1], XUEFENG YIN[1,2], (Member, IEEE), CHAO ZHANG[3], AND HAOWEN WANG[4]

[1]College of Electronics and Information Engineering, Tongji University, Shanghai 201804, China
[2]National Computer and Information Technology Practical Education Demonstration Center, Tongji University, Shanghai 201804, China
[3]APMS Section, Department of Electronic Systems, Faculty of Engineering and Science, Aalborg University, 9220 Aalborg, Denmark
[4]Shanghai Research Center for Wireless Communications, Shanghai 200050, China

Corresponding author: Xuefeng Yin (yinxuefeng@tongji.edu.cn)

This work was supported in part by the China National Science Foundation General Project under Grant 61971313, and in part by the National Science and Technology Major Project under Grant 2018ZX03001031-003.

ABSTRACT This paper presents a measurement-based analysis of wideband 39 GHz millimeter wave (mm-wave) dual-polarized propagation channel under the impact of foliage presence between a transmitter (Tx) and a receiver (Rx). The measurements were conducted in a rich-vegetation area, and the so-called direction-scan-sounding (DSS) method which rotates a horn antenna in angular domains was applied, aiming at investigating the direction-of-arrival (DoA)-dependent characteristics of polarimetric channels. Four Tx-to-Rx polarization configurations were considered, including co-polarization scenarios with vertical Tx-polarization to vertical Rx-polarization (VV) and horizontal to horizontal (HH), as well as cross-polarization with vertical to horizontal (VH) and horizontal to vertical (HV), which allow scrutinizing the differences in delay-direction dispersion for usually-encountered scenarios. A foliage loss model for various vegetation depths in VV polarization configuration, was also presented in this paper. The results show that the foliage-loss DoA spectra for VH and HV are similar, while the spectra exhibit less penetration loss in most directions for VV than for the HH. Furthermore, the presence of vegetation between the Tx and the Rx leads to larger dispersion in delay compared to the clear line-of-sight (LoS) scenario, particularly for vertical polarization in the Tx side, and additionally, the foliage presence also results in evident DoA dispersion, specially in the HV scenario. Selectivity in directions caused by foliage is more significant in vertically-polarized Tx scenarios than in the horizontally-polarized Tx scenarios. A statistical model is established summarizing these comparison details.

INDEX TERMS Millimeter-wave, 39 GHz, foliage attenuation, delay spread, angular spread, polarimetric characterization.

I. INTRODUCTION

With the exponentially increasing interests on the fifth-generation (5G) communication, the characteristics of millimeter-wave (mm-wave) propagation channel drew tremendous attention world-widely. Compared to the lower frequency bands, the range of wavelength for mm-wave frequency band reduces to the order of mm, and according to the attenuation caused by atmospheric absorption and precipitation through air increases drastically [1]. To combat with the high losses in mm-wave communications, high-gain directional antennas with narrow half-power-beamwidth (HPBW) were used in radio frequency (RF) signal transceiving for mm-wave channel sounding [2]–[6]. In addition, a so-called "directional scanning sounding (DSS)" method by rotating the axis of such antennas towards different directions was used in channel measurements to investigate channel dispersion in the direction domain.

The wave propagation through vegetation is common for wireless communications in outdoor environments. Many observations have shown that the presence of vegetation influences the quality of mm-wave communication due to

The associate editor coordinating the review of this manuscript and approving it for publication was Ke Guan.

severe penetration loss, rich scattering and significant de-polarization effects [7]–[9]. In most cases, vegetation has a significant influence on high frequency radio propagation since the attenuation through the vegetation is more severe in mm-wave bands than that in centimeter-wave (cm-wave) bands [10], [11]. However, the opposite observation was found in [12]. As the frequency of the measurement signal increases, the expected trend of increased attenuation values is not always evident for all foliage analyzed. Thus, it's worthwhile to analyze the attenuation through the vegetation. A so-called ''foliage attenuation'' which is defined as the power loss per unit length while waves propagate through the vegetated area in addition to the free space path loss was adopted to characterize the influence of vegetation [13].

Recently, many measurement campaigns have been performed to investigate the impact of vegetation on propagation channel characteristics for the cm-wave cases [14]–[19] and for mm-wave scenarios [20]–[23]. For example, a measurement campaign in outdoor scenarios for the foliage-affected wide-band channel at 73 GHz was conducted in [20], and for both co- and cross-polarized antenna configurations, the propagation attenuation was measured to be 0.4 dB/m. Foliage loss in vegetated areas which was associated with a saturating trend with upper-bounded foliage attenuation at 28 GHz was exhibited in [21]. Several frequency-dependent models such as the Internet Telecommunication Union Radiocommunication (ITU-R) model as well as the proposed model were presented to fit the measurement results. For a fixed frequency, foliage attenuation was found to depend on the leaf size, foliage density and other foliage parameters [22]. The propagation attenuation of isolated trees with different polarizations at 35, 94, and 140 GHz was characterized and presented in [23].

For polarization aspect, the existing works in [24]–[33] have provided valuable insights. In [24], both theoretical studies and indoor measurements for Rx with either vertical or horizontal polarizations and 12 Tx polarization orientations were conducted to explore the channels' polarimetric properties. As shown in [25], 60 GHz polarimetric directional indoor measurement results were applied to modifying and calibrating a 3D ray-tracing model. From the measurement results, it was found that perfect polarization matching can improve the system performance. In [26], channel measurement results on polarimetric characteristics of 60 GHz mm-wave channel has been reported which shows that the power degradation due to polarization mismatch can be up to 20 dB. A measurements with three kinds of polarimetric signal at 60 GHz were conducted in [27]. The results showed that the wave intensity depends on the specific polarization, and that the cross-polarized components was usually weak compared to the co-polarized components. Examples of narrowband polarimetric channel modeling shown in [31]–[33] demonstrated that the cross-polarization discrimination (XPD) is sensitive to the receiver's orientation, azimuthal spread and environment de-polarization behavior.

From the literature above, there is a lack of experimental studies specifically directed to vegetation attenuation in the mm-wave frequency band such as 39 GHz which has been considered for spectrum allocation bands of 5G Network. Besides, as far as we are concerned, the vegetation attenuation with respect to wave polarization at mm-wave frequencies has not been thoroughly investigated. Hence, filling the gaps particularly for the coverage of mm-wave-based 5G in enhanced mobile broadband (eMBB) applications is important. In this contribution, measurement and modeling have been conducted to explore millimeter-wave channel characterization under the impact of trees and polarization at 39 GHz with 2 GHz bandwidth. The contributions of the study presented here are listed in the following aspects:

1) Based on the directional dual-polarimetric wide-band channel measurements, we thoroughly analyze the influences of the vegetation and the Tx-Rx polarization combination on the mm-wave channel characteristics.
2) The relationship between the direction-dependent polarimetric channel characteristics and the foliage in the real measurements is presented, which is of significance for beamforming techniques.

The rest of this paper is organized as follow. In Section II, the measurement equipments and the measurement scenario are presented. In Section III, the signal model and channel characterization parameter are introduced. The power azimuth-elevation spectra of the polarimetric channels are reported in Section IV, together with the characteristics of the foliage loss, delay spread, angular spread and polarization parameters. Finally, conclusion remarks are addressed in Section V.

II. MEASUREMENT EQUIPMENT, AND SCENARIOS

A. MEASUREMENT EQUIPMENT

The channel sounding equipment applied in the measurement is composed of a programmable network analyser (PNA) and necessary auxiliaries. Diagram of the channel sounder is depicted in Figure 1. On the transmitter side of the sounder, the PNA is applied to generating signals at 6-8 GHz, resulting the bandwidth and center frequency equal to 2 GHz and 7 GHz, respectively. The number of frequency points swept in each snapshot is 1001, and the transmission power of the baseband signal is 39 dBm after being amplified by using a low frequency amplifier (LFAMP). Then the signal is modulated with a frequency-doubled local oscillator (LO) signal at 32 GHz. The signal is further amplified by a high frequency amplifier (HFAMP) with a gain of 30 dB and transmitted through the Tx antenna. On the receiver side, the incident signal is first amplified by the low noise amplifier (LNA) and then demodulated with the frequency-doubled LO signal. Note that the two LOs is connected with a cable for synchronization. Finally, the 2 GHz baseband channel transfer functions are stored for post processing. With a sensitivity of -110 dBm of the PNA, the overall dynamic range of the sounder is approximately 125 dB.

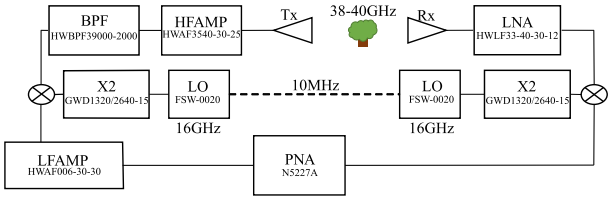

FIGURE 1. Diagram of the millimeter-wave directional channel sounder.

(a) The photograph of the measurement scenario.

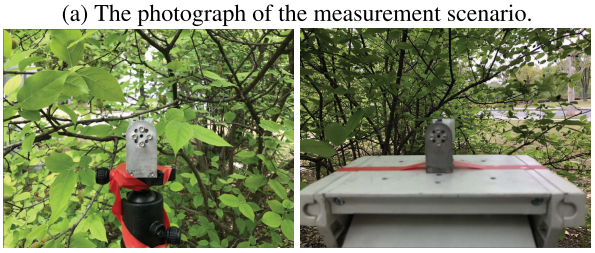

(b) View taken from Tx to Rx. (c) View taken from Rx to Tx.

FIGURE 2. Photographs of the measurement scenario and the views from the Tx to the Rx side and vice versa.

B. MEASUREMENT SCENARIOS A

The measurements for characterizing the influence of antenna polarization on foliage loss were conducted in Tongji University, Shanghai. Figure 2 shows the photograph of the measurement scenario and the view taken from the Tx to the Rx and vice versa during the measurements. The measured object is a plum tree near the road. In this scenario, the heights of the Tx and the Rx were both 1.5 m. The distance between the Tx and the Rx was 2.85 m, and the foliage exists between the Tx and the Rx. During the measurements, a DSS measurement scheme was employed with two identical 20° HPBW horn antennas equipped for both Tx and Rx sides. The Tx antenna was fixed, while the bore-sight of the Rx was set to rotate in azimuth within the range of $[-60°, 55°]$ and in elevation from $-30°$ to $30°$ in step of $5°$, which results in 24 steps in azimuth and 13 steps in elevation i.e. 312 steps in total for one measurement. We adjust the polarization configuration after each measurement, i.e., total four Tx-Rx antenna polarization configurations including co-polarized vertical-to-vertical (VV), co-polarized horizontal-to-horizontal (HH) antenna, cross-polarized vertical-to horizontal (VH) and cross-polarized horizontal-to-vertical (HV) were obtained. For fair comparison purposes,

TABLE 1. Measurement settings and specifications.

Parameter	Settings	Parameter	Settings
Antenna Type	Horn	HPBW [deg]	20
Gain [dBi]	15	XPI [dBi]	20
Transmit Power [dBm]	9	Dynamic Range [dB]	125
Azimuth [deg]	-60:5:55	Elevation [deg]	-30:5:30
Frequency Span [GHz]	38-40	Frequency Point	1001
Scenario A			
Tx-Rx Distance [m]	2.85	Antenna Height[m]	1.5
Scenario B			
Tx-Rx Distance [m]	2.85:11.8	Antenna Height[m]	1.5

FIGURE 3. A satellite view of measurement environment. The considered scenario is in an open place with many trees.

clear line-of-sight (LoS) measurements without obstacles existing between the Tx and the Rx with the same Tx and Rx polarization settings were also carried out. Table 1 summaries the configurations applied in these measurements.

C. MEASUREMENT SCENARIO B

The measurements for characterizing the influence of vegetation depth on foliage loss were conducted in the same area of the scenario A. Figure 3 shows the Tx and the Rx positions in the measurement scenario. In this scenario, the heights of the Tx and the Rx were the same as those in Scenario A. In these measurements, the Tx was fixed at the red point shown in Figure 3, while Rx was placed at several different positions in the rectangular area, which allows conducting measurements with vegetation depths ranging from 2.85 m to 11.8 m, under VV polarization. For fair comparison purposes, LoS measurements without obstacles existing between the Tx and the Rx were also carried out. Table 1 also summaries the configurations applied in Scenario B.

III. CHANNEL CHARACTERIZATION

A. GENERIC CHANNEL MODEL

In this study, we consider the multi-path Components (MPCs) in channel being characterized by complex-valued amplitude, propagation delay and direction-of-arrival (DoA). The noise-free channel impulse response (CIR) $h(t)_{p_{\mathrm{RX}},p_{\mathrm{TX}}}$ with

Rx polarization p_{Rx} and Tx polarization p_{Tx} can be written as

$$h(t)_{p_{\mathrm{Rx}},p_{\mathrm{Tx}}} = \sum_{\ell=1}^{L} \mathbf{A}_{\ell,p_{\mathrm{RX}},p_{\mathrm{TX}}} \delta\left(t-\tau_\ell\right) c(\Omega_\ell), \tag{1}$$

where L represents the number of MPCs, $\delta(\cdot)$ denotes the delta function, $\mathbf{A}_\ell$, τ_ℓ and Ω_ℓ represent the complex polarization matrix, the delay and the DoA set of the ℓth MPC, respectively. The complex polarization matrix $\mathbf{A}_\ell$ is written as

$$\mathbf{A}_\ell = \begin{bmatrix} \alpha_{\ell,\theta,\theta} & \alpha_{\ell,\theta,\phi} \\ \alpha_{\ell,\phi,\theta} & \alpha_{\ell,\phi,\phi} \end{bmatrix}, \tag{2}$$

where $\alpha_{\ell,p_{\mathrm{RX}},p_{\mathrm{TX}}}$ with $p_{\mathrm{RX}}, p_{\mathrm{TX}} \in \{\theta, \phi\}$ represents the complex amplitude by the signal transmitted with specific Tx polarization and Rx polarization for the ℓth path [30]. It is also worth mentioning that Ω_ℓ being a unit vector can be written as $\Omega_\ell = \mathrm{e}(\theta, \phi) = [\sin\theta \cdot \cos\phi \quad \sin\theta \cdot \sin\phi \quad \cos\theta]$, where θ,ϕ denotes the elevation and the azimuth respectively.

B. PARAMETER DEFINITIONS

In this paper, we focus on characterising the polarimetric channel from four aspects, i.e., foliage loss, delay spread, angular spread, and direction-dependent XPD spectra. Their definitions are briefly revisited in the sequel.

1) FOLIAGE LOSS

We use "foliage loss" in this paper to represent the loss caused by the presence of the vegetation. The foliage loss L_v for a direction Ω can be calculated as

$$L_v(\Omega)[\mathrm{dB}] = P_{\mathrm{LoS,m}}(\Omega) - P_{\mathrm{NLoS,m}}(\Omega), \tag{3}$$

where $L_v(\Omega)$ denotes the foliage loss, $P_{\mathrm{LoS,m}}(\Omega)$ and $P_{\mathrm{NLoS,m}}(\Omega)$ represent the maximum power of the power delay profile (PDP) in the LoS and non-LoS (NLoS) scenarios observed at the specific direction Ω, respectively.

From the nomenclature in [34]–[37], a model with three parameters a, b, c can be applied to fitting the measured foliage loss, i.e.

$$L_v[\mathrm{dB}] = a \cdot f^b \cdot d_v^c, \tag{4}$$

where d_v represents the vegetation depth in meters, and f denotes the frequency in MHz.

2) DELAY SPREAD

In this contribution, a high-resolution parameter estimation (HRPE) algorithm, i.e., space-alternating generalized expectation-maximization (SAGE) is applied to estimate the delay and amplitude of the multipath in each snapshot. The algorithm can be considered as an iterative implementation of the maximum likelihood estimation (MLE) method, providing the approximates of the ML estimates of unknown parameters [38], [39]. The estimated delay and amplitude parameters using the SAGE method are used to calculate the root-mean-square (RMS) delay spread by taking the second central-moment of the PDP [40].

3) ANGULAR SPREAD

Angular spread considered in our case, is referred to as the azimuth of arrival (AoA) spread denoted with σ_ϕ and the elevation of arrival (EoA) spread represented by σ_θ. A widely adopted approach for calculating angular spreads is to take the minimum of the second-order central moments of the angular power spectrum obtained by rotating with [0°, 360°] in azimuth or [0°, 180°] in elevation [41]. However, in this paper, the DSS is conducted in a portion of a sphere, i.e. from −60° to 55° in azimuth range and −30° to 30° in elevation range. Thus, the AoA spread σ_ϕ in our contribution analogous to the delay spread is computed approximately as the second central-moment of the truncated azimuth power spectrum $p(\phi)$, i,e.

$$\sigma_\phi \approx \sqrt{\frac{\Sigma_j(\phi_j - \mu_\phi)^2 \cdot p(\phi_j)}{\Sigma_j p(\phi_j)}}, \tag{5}$$

with the mean azimuth μ_ϕ calculating as,

$$\mu_\phi = \frac{\Sigma_j \phi_j \cdot p(\phi_j)}{\Sigma_j p(\phi_j)}, \tag{6}$$

where j is the index of the steps for scanning the azimuth range of interest.

For the EoA spread σ_θ, (5) and (6) can be used by replacing ϕ with θ.

4) DIRECTION-DEPENDENT POLARIMETRIC CHARACTERISTICS

Cross-polar discrimination (XPD) is an essential polarimetric parameter to describe channel polarimetric properties [32]. $\mathrm{XPD_H}(\Omega)$ is calculated as the direction-dependent power ratio of HH to HV in the direction Ω in decibel scale

$$\mathrm{XPD_H}(\Omega) = 10\log_{10}\left(\frac{P_{H,H}(\Omega)}{P_{H,V}(\Omega)}\right), \tag{7}$$

with

$$P_{H,H}(\Omega) = \int_0^T |h_{H,H}(\tau, \Omega)|^2 \mathrm{d}\tau,$$
$$P_{H,V}(\Omega) = \int_0^T |h_{H,V}(\tau, \Omega)|^2 \mathrm{d}\tau.$$

Similarly, $\mathrm{XPD_V}(\Omega)$ is referred to the direction-dependent power ratio of VV to VH in decibel

$$\mathrm{XPD_V}(\Omega) = 10\log_{10}\left(\frac{P_{V,V}(\Omega)}{P_{V,H}(\Omega)}\right), \tag{8}$$

with

$$P_{V,V}(\Omega) = \int_0^T |h_{V,V}(\tau, \Omega)|^2 \mathrm{d}\tau,$$
$$P_{V,H}(\Omega) = \int_0^T |h_{V,H}(\tau, \Omega)|^2 \mathrm{d}\tau,$$

where T represents the maximum length of the observed PDP.

Then, the so-called "polarimetric directional-dependent XPD spectra" (PDXS) can be drawn. The PDXS overlapped with the environments in the real measurement scenario

allow to investigate the relationship between XPD at specific direction and the foliage presence status, such as density and blockage level. Furthermore, these spectra can be used to compare the amplitude of vertical and horizontal PDXS. These properties reveal the direction-selectivity of the polarization. For better description and comparison of PDXS, a simple and robust cluster-extracting method is proposed in this contribution. This method consists of three steps: *Step I*, XPD thresholds above which a cluster is identified are empirically set to be 5 dB above the average XPD in each PDXS. *Step II*, the determined thresholds are applied to extract the dominant portions of the clusters that are larger than the threshold in two PDXSs. *Step III*, with the information of physical scatterers in the real measurement environments, the distinctions between the two PDXS at specific directions are studied and their relationships with the exact objects in the foliage are analyzed.

IV. EXPERIMENTAL RESULTS

In this section, polarimetric channel characteristics in the foliage NLoS scenario are analyzed from the perspectives of calculated the parameters, including the foliage loss, delay spread, angular spread and direction dependent XPD characteristics. For comparison reason, the channel characteristics in the LoS scenario are also illustrated.

A. POWER SPECTRA AND FOLIAGE LOSS

Figure 4 depicts the power azimuth-elevation of arrival spectra $\mathbf{P}(\Omega)$ of the channel observed when trees exist between the Tx and the Rx. The received power is mainly concentrated in the center of the spectra. However, the power distribution and the magnitude in the four spectra are different. From Figure 4(a), the power in $\mathbf{P}_{\mathrm{VV}}(\Omega)$ spreads from $-40°$ in azimuth to 25° and from $-30°$ to 30° in elevation, while for $\mathbf{P}_{\mathrm{HH}}(\Omega)$ shown in Figure 4(b) from $-50°$ to 10° in azimuth and from $-30°$ to 30° in elevation. For the cross-polarized power spectra $\mathbf{P}_{\mathrm{HV}}(\Omega)$ and $\mathbf{P}_{\mathrm{VH}}(\Omega)$ in Figure 4(c) and Figure 4(d), it can be observed that the received power of both spectra spreads similarly from $-35°$ to 15° in azimuth and from $-30°$ to 30° in elevation. In addition, the received power in $\mathbf{P}_{\mathrm{VV}}(\Omega)$, $\mathbf{P}_{\mathrm{HH}}(\Omega)$, $\mathbf{P}_{\mathrm{HV}}(\Omega)$ and $\mathbf{P}_{\mathrm{VH}}(\Omega)$ ranges within $[-64.3, -31.0]$ dB, $[-63.2, -30.5]$ dB, $[-70.1, -37.4]$ dB and $[-75.6, -43.1]$ dB, respectively, i.e. of dynamic range of 33.3 dB, 32.7 dB, 32.7 dB and 32.5 dB, correspondingly. It is obvious that the received power range in the two co-polarized power spectra i.e. $\mathbf{P}_{\mathrm{HH}}(\Omega)$ and $\mathbf{P}_{\mathrm{VV}}(\Omega)$ are similar. For the cross-polarized power spectra i.e. $\mathbf{P}_{\mathrm{HV}}(\Omega)$ and $\mathbf{P}_{\mathrm{VH}}(\Omega)$, the received power in the former is 5 dB higher than that in the latter. Besides, it is interesting to observe that there is no similarity between these two cross-polarized received powers. It indicates the vegetation impacts due to the extension of the branches and leaves on polarization are distinctive in our case.

The foliage loss spectra $\mathbf{L}_v(\Omega)$ with respect to different combinations of the polarizations are shown in Figure 5. From the co-polarized $\mathbf{L}_v(\Omega)$ in Figure 5(a) and Figure 5(b),

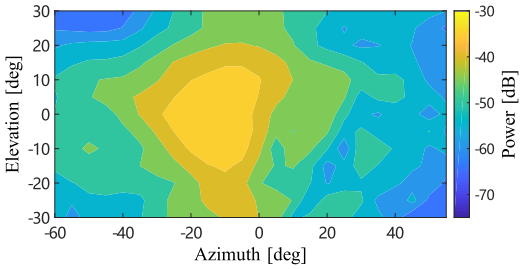

(a) Vertical to vertical

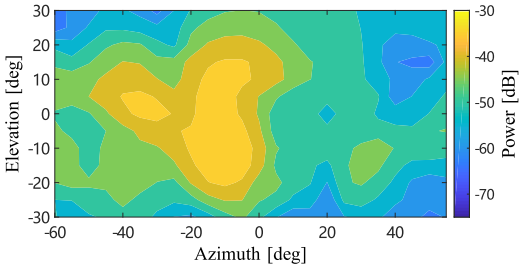

(b) Horizontal to horizontal

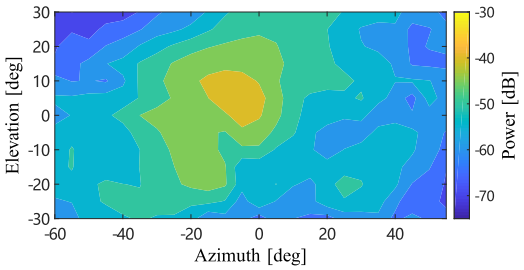

(c) Horizontal to vertical

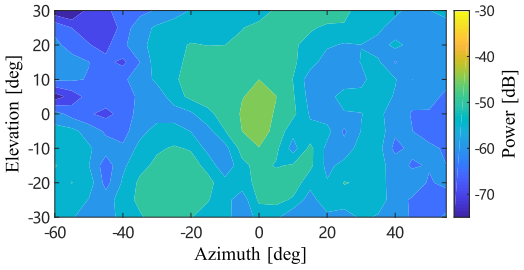

(d) Vertical to horizontal

FIGURE 4. The azimuth-elevation power spectra under different configurations of polarization in foliage NLoS scenario.

both co-polarized foliage loss are similar in the area enclosed by a red oval frame. Besides, the foliage loss of HH is much higher than that of VV in the area enclosed by a black oval frame, where the foliage are thin. From the cross-polarized $\mathbf{L}_v(\Omega)$ in Figure 5(c) and Figure 5(d), the value of $\mathbf{L}_{v,HV}(\Omega)$ in the area enclosed by a red oval frame is higher than the value of $\mathbf{L}_{v,VH}(\Omega)$. The maximum value $L_{v,\mathrm{m}}$ of $\mathbf{L}_v(\Omega)$ and the mean value $\overline{L}_v$ of $\mathbf{L}_v(\Omega)$ are illustrated in Table 2. We observe that $L_{v,\mathrm{m,VV}}$ is 5.3 dB less than $L_{v,\mathrm{m,HH}}$, and for cross-polarization VH and HV, the maximum values of foliage loss spectra are nearly the same. As for the mean value $\overline{L}_v$, we found that $\overline{L}_{v,HH}$ is 1.6 dB higher than $\overline{L}_{v,VV}$. Besides, for cross-polarization VH and HV, it is interesting to observe that

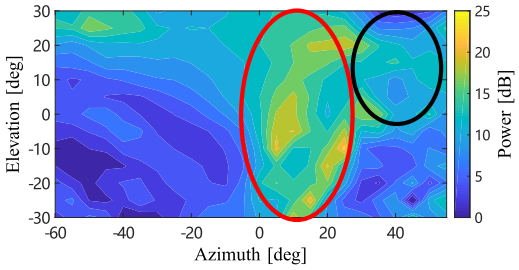

(a) Vertical to vertical

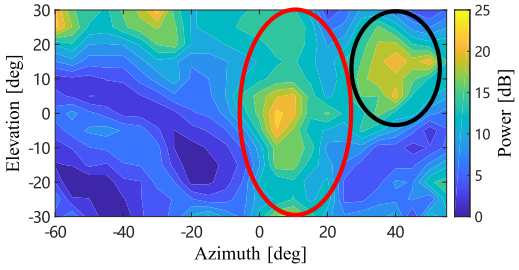

(b) Horizontal to horizontal

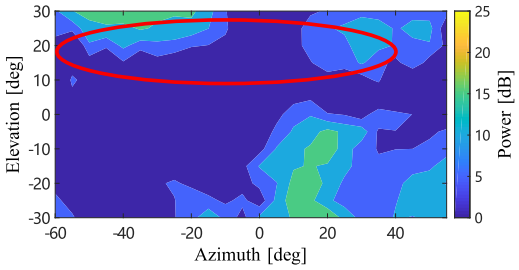

(c) Horizontal to vertical

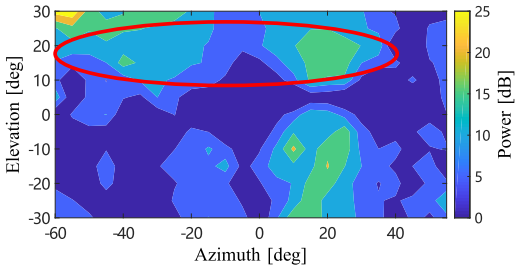

(d) Vertical to horizontal

FIGURE 5. The azimuth-elevation foliage loss spectra under different configurations of polarization.

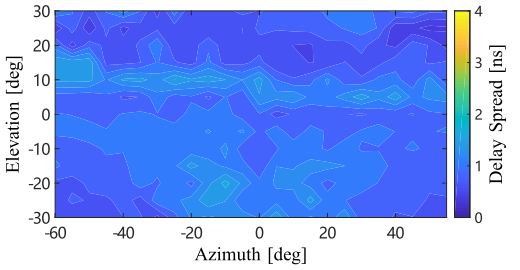

(a) Vertical to vertical

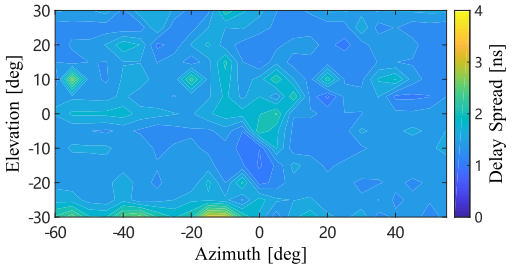

(b) Horizontal to horizontal

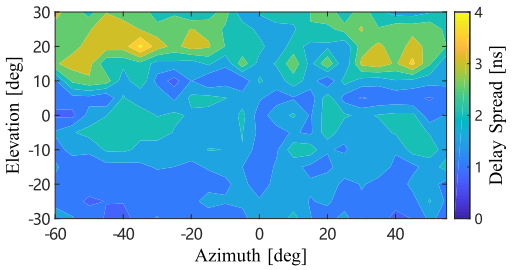

(c) Horizontal to vertical

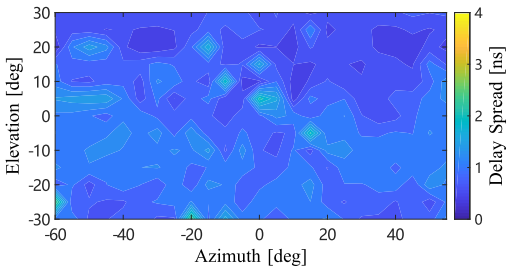

(d) Vertical to horizontal

FIGURE 6. The azimuth-elevation delay spread spectra under different configurations of polarization in LoS scenario.

the two $\overline{L}_v$s are negative, which, according to our postulation, is caused by the polarization transition or dispersion when wave traverses through the vegetation. From the observations above, it is evident that the vertical polarization has less vegetation penetration loss than that obtained for horizontal polarization.

Foliage loss models were investigated in [34]–[37]. Based on the widely adopted model $L_v[\text{dB}] = a \cdot f^b \cdot d_v^c$ and measurement data obtained in Scenario B, the least square method was adopted for determining the parameter values. The obtained model is written as

$$L_v[\text{dB}] = 2.143 \cdot f^{0.078} \cdot d_v^{0.650}, \tag{9}$$

B. CHANNEL DELAY SPREAD WITH RESPECT TO POLARIZATION

Figures 6 and 7 depict the delay spread spectra $\Gamma(\Omega)$ calculated under different configurations of polarization in the foliage LoS and the NLoS scenarios, respectively. As illustrated in Figure 6 and 7, the delay spreads in the LoS scenario vary in the range of 1.0-3.5 ns, while all the delay spreads in the NLoS scenario of the four spectra increase to [1.02, 7.73] ns in HH, [1.32, 7.72] ns in VV, [1.11, 9.52] ns in HV and [1.10, 10.26] ns in VH, respectively. Obviously, the dynamic ranges of the cross-polarimetric NLoS delay spreads are much higher than those of co-polarimetric NLoS delay spreads. As illustrated in Figure 7, some of the values

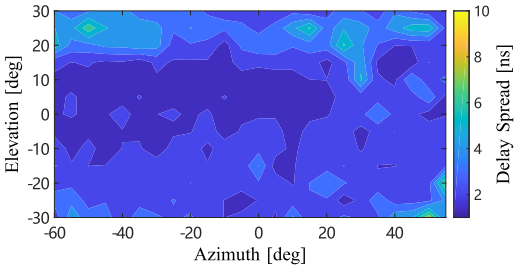

(a) Vertical to vertical

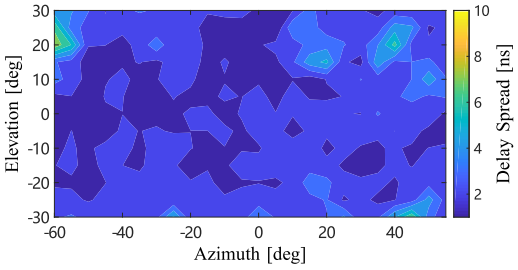

(b) Horizontal to horizontal

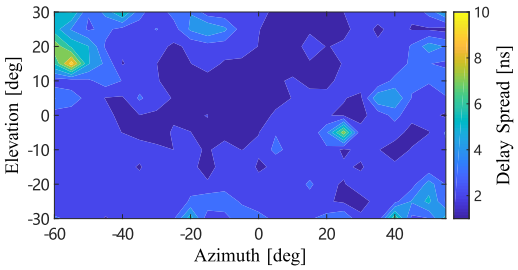

(c) Horizontal to vertical

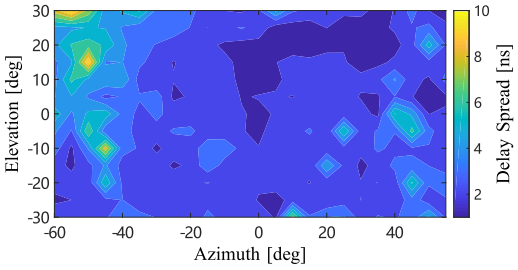

(d) Vertical to horizontal

FIGURE 7. The azimuth-elevation delay spread spectra under different configurations of polarization in foliage NLoS scenario.

at the edge of the spectra are much higher than those in the central region, such phenomena are caused by the multipath richness at the edge. In order to explain the difference of the dealy spread value at central and edge position, we compared two relative PDPs of HH polarimetric channel at the 0° azimuth and the 0° elevation (0°, 0°) and the −60° azimuth and the 25° elevation (−60°, 25°) in Figure 8. It can be observed from Figure 8 that the latter relative PDP has many long delay multipath components, while the former relative PDP drops more smoothly. Furthermore, the latter relative PDP has sharper fluctuations in 20-100 ns. This phenomenon is caused by the fact that when the axis of the horn antenna deviates largely from the LoS orientation, the distribution of

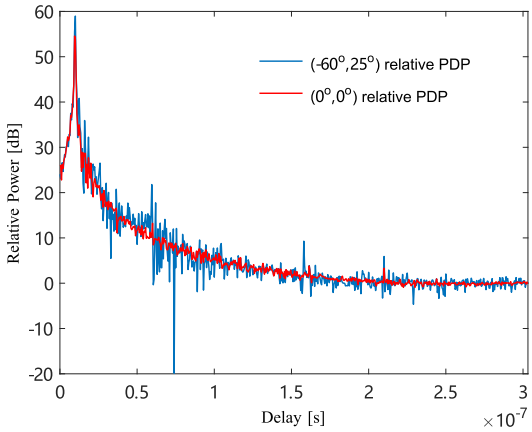

FIGURE 8. Comparison of relative PDP and estimated value of the center and the edge of HH polarization.

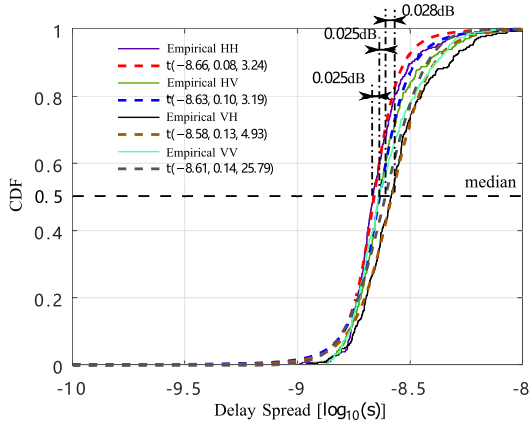

(a) CDF for NLoS

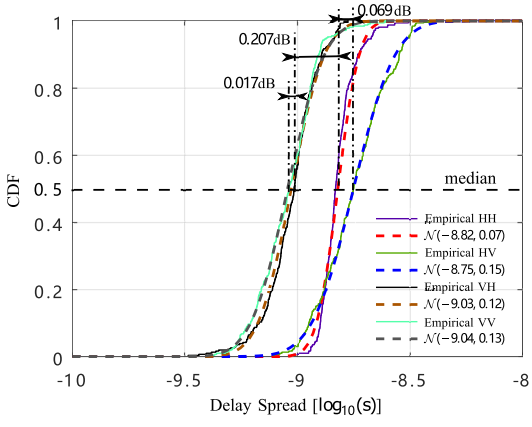

(b) CDF for LoS

FIGURE 9. The CDF of delay spreads in the foliage NLoS and the LoS scenarios.

the foliage along the axis of the antenna becomes increasingly denser than that along LoS orientation.

The cumulative probability function (CDF) of delay spread in the foliage NLoS and the LoS scenarios are shown in Figure 9, while the statistics of the delay spread are illustrated in Table 2. All the delay spreads' CDF of four

TABLE 2. Summary of the experimental results of channel parameters.

Tx-Rx Polarization Config.	VV	VH	HV	HH
Foliage Loss				
$L_{v,max}$ [dB]	20.8	22.9	22.0	26.1
$\overline{L_v}$ [dB]	10.5	-3.1	-5.6	12.1
Delay spread				
Scenario	NLoS			
μ [dB]	-8.61	-8.58	-8.63	-8.66
σ	0.14	0.13	0.10	0.08
γ	25.79	4.93	3.19	3.24
Scenario	LoS			
μ [dB]	-9.04	-9.03	-8.75	-8.82
σ	0.13	0.12	0.15	0.07
Median Difference [dB]	0.43	0.45	0.12	0.16
AoA and EoA spread				
Scenario	NLoS			
AoA Spread [deg]	15.2	23.5	19.9	18.1
EoA Spread [deg]	11.4	17.3	13.8	11.8
Scenario	LoS			
AoA Spread [deg]	13.9	22.0	23.5	17.2
EoA Spread [deg]	11.5	19.6	18.5	12.4
AoA Difference [deg]	1.3	1.5	-3.6	0.9
EoA Difference [deg]	-0.1	-2.3	-4.7	-0.6

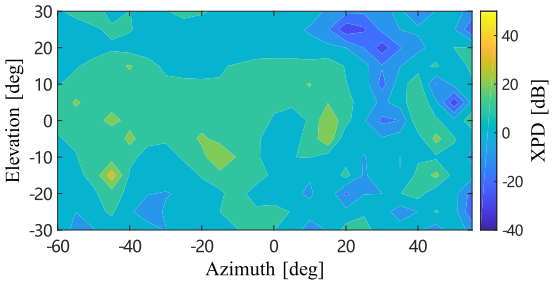

(a) The vertical PDXS

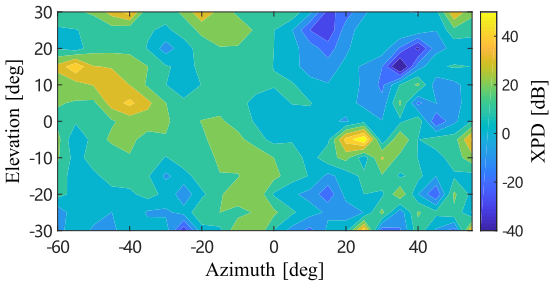

(b) The horizontal PDXS

FIGURE 10. The PDPSs under vertical and horizontal polarization.

polarization configuration can be well-fitted with the T location-scale distribution. However, all the delay spreads' CDF in LoS scenario are well-fitted with the normal distribution. All of the NLoS delay spreads are statistically higher than those in the LoS scenario. In the LoS scenario, Figure 9(b) demonstrates that the delay spreads under VV and VH conditions are 0.207 dB statistically lower than those under HH and HV conditions. It is worth mentioning that in Figure 6, the delay spreads under HH and HV conditions are also observed to be higher than those under VV and VH conditions in most regions, which according to our postulation, is due to the asymmetry of the openness of obstacles along the LoS direction. In the NLoS scenario, the delay spreads of VV and VH conditions reach the values of -8.61 dB and -8.58 dB which are closed to the delay spreads of the HH and the HV conditions. Furthermore, comparing the difference between the delay spreads in the LoS and the NLoS scenarios, the VV difference of 0.43 dB and the VH difference of 0.45 dB are much higher than the HH difference of 0.16 dB and the HV difference of 0.12 dB. In the foliage NLoS scenario, it is obvious that the vertical polarization in the transmitting side has an innegligible influence on delay spread. Our conclusion is that the presence of the trees leads to large dispersion in the delay domain and the polarization of the Tx antenna has an significant increase on delay spread.

C. CHANNEL ANGULAR SPREAD WITH RESPECT TO POLARIZATION

Table 2 also contains the AoA and the EoA spread in the foliage NLoS and the LoS scenarios. All of the angular spreads are varied within a small scope due to the short Tx-Rx distance. Comparing the AoA and EoA spreads in the LoS and NLoS scenarios, the following observations can be obtained: *i)* Under co-polarization conditions, the VV AoA spread enlarges from 13.9° to 15.2° in the NLoS scenario compared to that in the LoS scenario. However, no significant change has been found in the VV EoA spread. Besides, under HH condition, the NLoS AoA spread increase 0.9° when comparing with the LoS AoA spread, while the NLoS EoA spread decreases from 12.4° to 11.8°; *ii)* Under cross-polarization conditions, the HV AoA spread in the LoS scenario is 23.5°, then it decreases to 19.9° in the NLoS scenario, and the HV EoA spread decreases from 18.5° to 13.8° when vegetation appear. Under VH condition, the AoA spread enlarges from 22.0° to 23.5° in the NLoS scenario compared to that in the LoS scenario. On the contrary, vegetation attenuation leads to a 2.3° reduction of EoA spread. These results imply explicitly that the co-polarized AoA spreads in the NLoS scenario are larger than those obtained in the LoS scenario, and that the co-polarized EoA spreads in the NLoS scenario are less than those observed in the LoS scenario. For the cross-polarization scenarios, most of the angular spreads are small compared to their co-polarization counterparts. In addition, the AoA and EoA spreads under the HV configuration exhibit the largest difference of 3.6° and 4.7°, respectively, compared to those in the LoS scenarios.

D. DIRECTION-DEPENDENT XPD CHARACTERISTICS

Figure 10 depicts the PDXSs of $\mathrm{XPD_H}$ and $\mathrm{XPD_V}$. Figure 11 illustrates the CDFs of the vertical and horizontal XPD. From the plots, it can be observed that the values of $\mathrm{XPD_H}$ and of $\mathrm{XPD_V}$ range from -47.59 dB to 59.69 dB and from -27.64 dB to 35.61 dB, respectively, with dynamic ranges of 107.28 dB and of 63.25 dB, respectively. Obviously,

TABLE 3. Comparison of foliage loss models.

Model	Formulation	Conditions	RMSE[dB]
Fitted model	$L_v[\text{dB}] = 2.143 \cdot f^{0.078} \cdot d_v^{0.650}$	38 GHz $\leq f \leq$ 40 GHz, f in MHz	5.79
COST 235 [34]	$L_v[\text{dB}] = 13.77 \cdot f^{-0.009} \cdot d_v^{0.26}$	in-leaf, $d_v \leq 200$ m, 9.6 GHz $\leq f \leq$ 57.6 GHz	9.16
ITU-R [35]	$L_v[\text{dB}] = 0.25 \cdot f^{0.39} \cdot d_v^{0.25} \cdot \theta^{0.05}$	30 MHz $\leq f \leq$ 60 GHz	6.35
FITU-R [36]	$L_v[\text{dB}] = 0.39 \cdot f^{0.39} \cdot d_v^{0.25}$	in-leaf, 10 GHz $\leq f \leq$ 40 GHz	22.8
Weissberger [37]	$L_v[\text{dB}] = 0.187 \cdot f^{0.284} \cdot d_v^{0.588}$	$f \leq$ 95 GHz	8.47

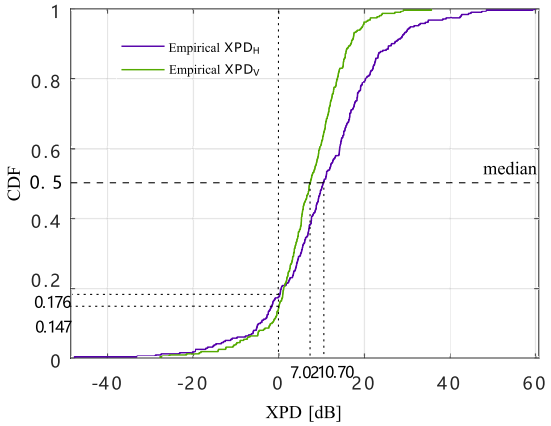

FIGURE 11. The CDF of XPD_H and XPD_V.

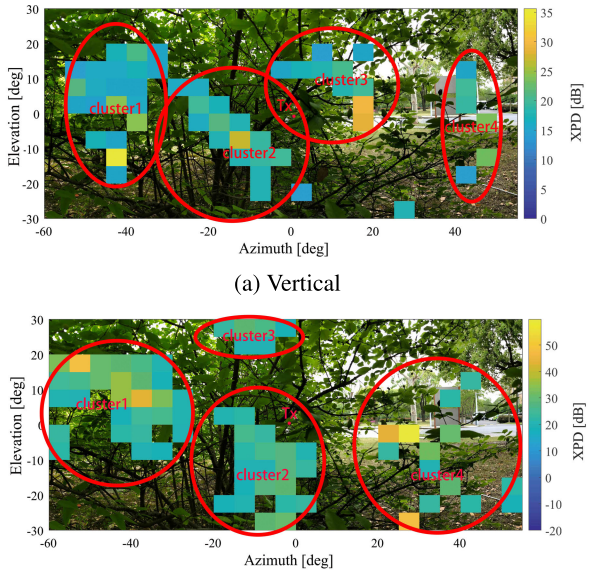

(a) Vertical

(b) Horizontal

FIGURE 12. The relationship spectra of XPD after clustering and real measurement scenario.

the dynamic range of XPD_V is less than XPD_H by almost 40 dB. The mean value $\overline{XPD}_H$ is 10.70 dB, which is 3.68 dB higher than $\overline{XPD}_V$. Besides, the percentage of XPD_V and XPD_H exceeding zero are 85.3% and 82.4%, respectively, which reveals that the co-polarized components' power is superior to the cross-polarized components in general with high probability. The relationship between the clusters identified in the XPD_V and XPD_H spectra and the foliage in the real measurement scenario is illustrated in Figure 12. Four clusters can be found for both XPD_V and XPD_H DoA spectra. From Figure 12(a) and 12(b), it is particularly observed that XPD cluster 1, 2 and 4 appear in the same location in the spectra. However, XPD_V cluster 3 appears at the center of Figure 12(a) while XPD_H cluster 3 appears at the top of Figure 12(b). The observations demonstrate that although the foliage channel may have similar directional selectivity towards differently polarized wave, distinction still exist in specific portions of the foliage.

E. MODEL SUMMARY AND COMPARISON TO EXISTING COUNTERPART

With regard to foliage loss, Table 3 compares our foliage loss model in terms of (9) with existing ones described in [34]–[37]. The exact formulation, the parameter values are also presented in Table 3. Furthermore, the predicted L_v are calculated and used to obtain the root-mean-square-error (RMSE) of the model prediction. According to our calculation, the model obtained here in our work performs the best with the minimum RMSE of 5.79 dB. The second-best fitted model is ITU-R model with RMSE of 6.35 dB, 0.56 dB larger than the model proposed here. It is obvious that our proposed model has a better applicability in describing the vegetation attenuation at 39 GHz.

To our best knowledge, no polarimetric foliage attenuation model has been found so far. As alternatives, we introduce several analogous foliage attenuation models in [33], [35], [42] for comparison. In the delay spread aspect, a cherry tree attenuation model under VV condition was presented in [35] where the vegetation depth is 6.2 m and the carrier frequency is 3.5 GHz with 0.78 GHz bandwidth. The mean value of the delay spread is 8.23 ns, which is significantly higher than the value found in our contribution. According to our postulation, this is due to the lower foliage attenuation in sub 6 GHz band. Moreover, a foliage attenuation model under VV condition was presented in [42] where the vegetation depth is 3.0 m and the carrier frequency is 39 GHz with 2 GHz bandwidth. The mean value of the delay spread is 2.6 ns which coincides with our results. In the aspects of XPD, the polarimetric channel characteristics XPD with different Tx-Rx distance at 3.8 GHz was illustrated in [33]. The range of XPD is within $[-1, 6]$ dB which is slightly lower than the mean values of the XPD_H and of the XPD_V discovered in our paper. This is due to the possible reason that 20° HPBW horn antennas and DSS method were adopted, resulting in higher spatial resolution for multipath detection. Furthermore, it is worth to emphasize that one of our contribution is the XPD characterised in the

directional domain, which as far as we are concerned, is the first of this kind of study.

V. CONCLUSION

This paper presented a measurement-based study of wideband 39 GHz mm-wave dual-polarimetric channel propagation through vegetation. A set of directional measurements under different polarization configuration using DSS method exploring the azimuth from $-60°$ to $55°$ and the elevations from $-30°$ to $30°$ were performed in a fixed scenario for the purpose of exploring the foliage loss, channel dispersive characteristics and polarization characteristic. A foliage loss model for various vegetation depths in VV polarization configuration, was also presented in this paper.

Preliminary conclusions have been drawn from the directional measurements we conducted. All the foliage loss spectra under four different polarization configuration are similar in directions. Comparing the maximum and mean value of the foliage loss spectra, the foliage loss of VV configuration is lower than that of HH, while for cross-polarization VH and HV, the foliage loss are nearly the same. It is natural to conclude that the vertical polarization has less severe vegetation penetration loss than horizontal. For dispersive characteristics, all the delay spread of four polarization combination in foliage NLoS scenario fit the T location-scale distribution. Significant difference of delay spreads and angular spreads are observed under different polarization configurations, and the polarization of the Tx antenna has an significant effect on delay spread. Besides, the comparison of the vertical and horizontal XPD show that the vertical polarization characteristics is more selective than horizontal polarization in direction when wave propagates through the vegetation. Compared with existing channel models, the proposed directional-dependent XPD in our contribution provides a more comprehensive polarization description in the spatial domain.

REFERENCES

[1] T. S. Rappaport, S. Sun, R. Mayzus, H. Zhao, Y. Azar, K. Wang, G. N. Wong, J. K. Schulz, M. Samimi, and F. Gutierrez, "Millimeter wave mobile communications for 5G cellular: It will work!" *IEEE Access*, vol. 1, pp. 335–349, May 2013.

[2] X. Yin, C. Ling, and M.-D. Kim, "Experimental multipath-cluster characteristics of 28-GHz propagation channel," *IEEE Access*, vol. 3, pp. 3138–3150, Apr. 2015.

[3] C. Ling, X. Yin, R. Müller, S. Häfner, D. Dupleich, C. Schneider, J. Luo, H. Yan, and R. Thomä, "Double-directional dual-polarimetric cluster-based characterization of 70–77 GHz indoor channels," *IEEE Trans. Antennas Propag.*, vol. 66, no. 2, pp. 857–870, Feb. 2018.

[4] X. Yin, Y. Ji, and H. Yan, "Measurement-based characterization of 15 GHz propagation channels in a laboratory environment," *IEEE Access*, vol. 5, pp. 1428–1438, 2017.

[5] X. Yin, L. Ouyang, and H. Wang, "Performance comparison of SAGE and MUSIC for channel estimation in direction-scan measurements," *IEEE Access*, vol. 4, pp. 1163–1174, 2016.

[6] M. Samimi, K. Wang, Y. Azar, G. N. Wong, R. Mayzus, H. Zhao, J. K. Schulz, S. Sun, F. Gutierrez, and T. S. Rappaport, "28 GHz angle of arrival and angle of departure analysis for outdoor cellular communications using steerable beam antennas in New York City," in *Proc. IEEE 77th Veh. Technol. Conf. (VTC Spring)*, Jun. 2013, pp. 1–6.

[7] F. Wang and K. Sarabandi, "An enhanced millimeter-wave foliage propagation model," *IEEE Trans. Antennas Propag.*, vol. 53, no. 7, pp. 2138–2145, Jul. 2005.

[8] I. J. Dilworth and B. L'Ebraly, "Propagation effects due to foliage and building scatter at millimetre wavelengths," in *Proc. 9th Int. Conf. Antennas Propag. (ICAP)*, vol. 2, Apr. 1995, pp. 51–53.

[9] N. C. Rogers, A. Seville, J. Richter, D. Ndzi, and N. Savage, "A generic model of 1-60 GHz radio propagation through vegetation-final report," Radio Agency, London, U.K., Tech. Rep. QINETIQ/KI/COM/CR020196/1.0, 2002.

[10] J. E. J. Dalley, M. S. Smith, and D. N. Adams, "Propagation losses due to foliage at various frequencies," in *Proc. IEE Nat. Conf. Antennas Propag.*, Apr./Mar. 1999, pp. 267–270.

[11] H. M. Rahim, C. Y. Leow, T. A. Rahman, A. Arsad, and M. A. Malek, "Foliage attenuation measurement at millimeter wave frequencies in tropical vegetation," in *Proc. IEEE 13th Malaysia Int. Conf. Commun. (MICC)*, Nov. 2017, pp. 241–246.

[12] T. R. Fernandes, R. F. Caldeirinha, M. Al-Nuaimi, and J. Richter, "A discrete RET model for millimeter-wave propagation in isolated tree formations," *IEICE Trans. Commun.*, vol. 88, no. 6, pp. 2411–2418, 2005.

[13] I. Rodriguez, R. Abreu, E. P. L. Almeida, M. Lauridsen, A. Loureiro, and P. Mogensen, "24 GHz cmwave radio propagation through vegetation: Suburban tree clutter attenuation," in *Proc. 10th Eur. Conf. Antennas Propag. (EuCAP)*, Apr. 2016, pp. 1–5.

[14] R. Yoshimura, M. Hara, T. Nishimura, C. Yamada, H. Shimasaki, Y. Kado, and M. Ichida, "Effect of vegetation on radio wave propagation in 920-MHz and 2.4-GHz bands," in *Proc. Asia–Pacific Microw. Conf. (APMC)*, Dec. 2016, pp. 1–4.

[15] G. Durgin, T. S. Rappaport, and H. Xu, "Radio path loss and penetration loss measurements in and around homes and trees at 5.85 GHz," in *IEEE Antennas Propag. Soc. Int. Symp., Dig. Antennas, Gateways Global Netw. Held Conjunct, USNC/URSI Nat. Radio Sci. Meeting*, vol. 2, Jun. 1998, pp. 618–621.

[16] P. Horak and P. Pechac, "Excess loss for high elevation angle links shadowed by a single tree: Measurements and modeling," *IEEE Trans. Antennas Propag.*, vol. 60, no. 7, pp. 3541–3545, Jul. 2012.

[17] A. Alsayyari, I. Kostanic, C. E. Otero, and A. Aldosary, "An empirical path loss model for wireless sensor network deployment in a dense tree environment," in *Proc. IEEE Sensors Appl. Symp. (SAS)*, Mar. 2017, pp. 1–6.

[18] K. Benzair, "Measurements and modelling of propagation losses through vegetation at 1-4 GHz," in *Proc. 9th Int. Conf. Antennas Propag. (ICAP)*, vol. 2, Apr. 1995, pp. 54–59.

[19] D. Reudink and M. Wazowicz, "Some propagation experiments relating foliage loss and diffraction loss at X-band and UHF frequencies," *IEEE Trans. Commun.*, vol. 21, no. 11, pp. 1198–1206, Nov. 1973.

[20] T. S. Rappaport and S. Deng, "73 GHz wideband millimeter-wave foliage and ground reflection measurements and models," in *Proc. IEEE Int. Conf. Commun. Workshop (ICCW)*, Jun. 2015, pp. 1238–1243.

[21] J. Ko, Y.-S. Noh, Y.-C. Kim, S. Hur, S.-R. Yoon, D. Park, K. Whang, D.-J. Park, and D.-H. Cho, "28 GHz millimeter-wave measurements and models for signal attenuation in vegetated areas," in *Proc. 11th Eur. Conf. Antennas Propag. (EUCAP)*, Mar. 2017, pp. 1808–1812.

[22] S. Joshi and S. Sancheti, "Foliage loss measurements of tropical trees at 35 GHz," in *Proc. Int. Conf. Recent Adv. Microw. Theory Appl.*, Nov. 2008, pp. 531–532.

[23] F. T. Ulaby, T. H. Haddock, and Y. Kuga, "Measurement and modeling of millimeter-wave scattering from tree foliage," *Radio Sci.*, vol. 25, no. 3, pp. 193–203, May 1990.

[24] X. Yin, Y. He, C. Ling, L. Tian, and Z. Zhong, "A preliminary study on anisotropic characteristics of propagation channels for Tx-Rx polarizations," in *Proc. IEEE Wireless Commun. Netw. Conf. (WCNC)*, Apr. 2013, pp. 3455–3459.

[25] V. Degli-Esposti, F. Fuschini, E. M. Vitucci, M. Barbiroli, M. Zoli, D. Dupleich, R. Müller, C. Schneider, and R. S. Thomä, "Polarimetric analysis of mm-wave propagation for advanced beamforming applications," in *Proc. 9th Eur. Conf. Antennas Propag. (EuCAP)*, May 2015, pp. 1–4.

[26] A. Maltsev, E. Perahia, R. Maslennikov, A. Sevastyanov, A. Lomayev, and A. Khoryaev, "Impact of polarization characteristics on 60-GHz indoor radio communication systems," *IEEE Antennas Wireless Propag. Lett.*, vol. 9, pp. 413–416, May 2010.

[27] H. Sawada, H. Nakase, S. Kato, M. Umehira, K. Sato, and H. Harada, "Polarization dependence in double directional propagation channel at 60 GHz," in *Proc. IEEE 20th Int. Symp. Pers., Indoor Mobile Radio Commun.*, Sep. 2009, pp. 3010–3014.

[28] D. Giuli, "Polarization diversity in radars," *Proc. IEEE*, vol. 74, no. 2, pp. 245–269, Feb. 1986.

[29] A. P. G. Ariza, R. Möller, F. Wollenschläger, A. Schulz, M. Elkhouly, Y. Sun, S. Glisic, U. Trautwein, R. Stephan, J. Müller, R. S. Thomä, and M. Hein, "60 GHz ultrawideband polarimetric MIMO sensing for wireless multi-gigabit and radar," *IEEE Trans. Antennas Propag.*, vol. 61, no. 4, pp. 1631–1641, Apr. 2013.
[30] X. Yin, Y. He, C. Ling, L. Tian, and X. Cheng, "Empirical stochastic modeling of multipath polarizations in indoor propagation scenarios," *IEEE Trans. Antennas Propag.*, vol. 63, no. 12, pp. 5799–5811, Dec. 2015.
[31] F. Quitin, C. Oestges, F. Horlin, and P. D. Doncker, "Multipolarized MIMO channel characteristics: Analytical study and experimental results," *IEEE Trans. Antennas Propag.*, vol. 57, no. 9, pp. 2739–2745, Sep. 2009.
[32] E. M. Vitucci, F. Mani, V. Degli-Esposti, and C. Oestges, "Polarimetric properties of diffuse scattering from building walls: Experimental parameterization of a ray-tracing model," *IEEE Trans. Antennas Propag.*, vol. 60, no. 6, pp. 2961–2969, Jun. 2012.
[33] F. Mani and C. Oestges, "A ray based method to evaluate scattering by vegetation elements," *IEEE Trans. Antennas Propag.*, vol. 60, no. 8, pp. 4006–4009, Aug. 2012.
[34] M. P. M. Hall, "COST Project 235 activities on radiowave propagation effects on next-generation fixed-service terrestrial telecommunication systems," in *Proc. 8th Int. Conf. Antennas Propag.*, vol. 2, Mar./Apr. 1993, pp. 655–659.
[35] *Attenuation in Vegetation*, document ITU-R P.833-9, 2016.
[36] M. O. Al-Nuaimi and R. B. L. Stephens, "Measurements and prediction model optimisation for signal attenuation in vegetation media at centimetre wave frequencies," *IEE Proc.-Microw., Antennas Propag.*, vol. 145, no. 3, pp. 201–206, Jun. 1998.
[37] M. A. Weissberger, "An initial critical summary of models for predicting the attenuation of radio waves by trees," Electromagn. Compat. Anal. Center, Annapolis, MD, USA, Tech. Rep. ESD-TR-81-101, 1982.
[38] B. H. Fleury, M. Tschudin, R. Heddergott, D. Dahlhaus, and K. Ingeman Pedersen, "Channel parameter estimation in mobile radio environments using the SAGE algorithm," *IEEE J. Sel. Areas Commun.*, vol. 17, no. 3, pp. 434–450, Mar. 1999.
[39] X. Yin and X. Cheng, *Propagation Channel Characterization, Parameter Estimation and Modeling for Wireless Communications*. Singapore: Wiley, 2016.
[40] C. Ling, X. Yin, H. Wang, and R. S. Thomä, "Experimental characterization and multipath cluster modeling for 13–17 GHz indoor propagation channels," *IEEE Trans. Antennas Propag.*, vol. 65, no. 12, pp. 6549–6561, Dec. 2017.
[41] B. H. Fleury, "First- and second-order characterization of direction dispersion and space selectivity in the radio channel," *IEEE Trans. Inf. Theory*, vol. 46, no. 6, pp. 2027–2044, Sep. 2000.
[42] C. Zhang, X. Yin, X. Cai, and Z. Yu, "Wideband 39 GHz millimeter-wave channel measurements under diversified vegetation," in *Proc. IEEE 29th Annu. Int. Symp. Pers., Indoor Mobile Radio Commun. (PIMRC)*, Sep. 2018, pp. 1–6.

YEJIAN LV received the bachelor's degree in electrical engineering and automation from Tongji University, Shanghai, China, in 2017, where he is currently pursuing the master's degree with the College of Electronics and Information Engineering. His research interests include statistical channel characterization, millimeter wave channel characterization, and modeling.

XUEFENG YIN (S'01–M'06) received the bachelor's degree in optoelectronics engineering from the Huazhong University of Science and Technology, Wuhan, China, in 1995, and the M.Sc. degree in digital communications and the Ph.D. degree in wireless communications from Aalborg University, Aalborg, Denmark, in 2002 and 2006, respectively, where he was an Assistant Professor, from 2006 to 2008. In 2008, he joined the College of Electronics and Information Engineering, Tongji University, Shanghai, China, where he became a Full Professor, in 2016, and has been the Vice Dean, since then. He has authored or coauthored more than 130 technical articles and coauthored the book *Propagation Channel Characterization, Parameter Estimation, and Modeling for Wireless Communications* (John Wiley & Sons, IEEE Edition, 2016). His research interests include high-resolution parameter estimation for propagation channels, measurement-based channel characterization and stochastic modeling for 5G wireless communications, channel simulation based on random graph models, and environment sensing based on millimeter-wave.

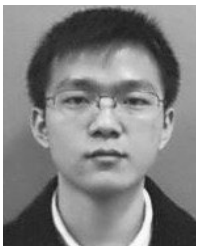

CHAO ZHANG received the B.S. and M.S. degrees in electronics science and technology from Tongji University, Shanghai, China, in 2013 and 2019, respectively. Since Novermber 2018, he has been an Intern with the APMS Section, Department of Electronic Systems, Aalborg University, Aalborg, Denmark. His research interests include measurement-based propagation channel characterization and modeling, development of high-resolution propagation parameter estimation algorithms, array signal processing, and OTA testing.

HAOWEN WANG is currently a Senior Engineer with the Shanghai Research Center for wireless communication and the Shanghai Institute of Microsystem and Information Technology, Chinese Academy of Sciences. He has many years of working experience in testing, measurement, and verification of advanced wireless communication technologies. His current research interests include RF data acquisition, channel measurement and modeling, and system-level wireless testbeds.